Carbon-incorporated nickel-cobalt mixed metal phosphide nanoboxes with enhanced electrocatalytic activity for oxygen evolution

He, Peilei; Yu, Xin-Yao; Lou, David Xiong Wen

2017

He, P., Yu, X.-Y., & Lou, D. X. W. (2017). Carbon-incorporated nickel-cobalt mixed metal phosphide nanoboxes with enhanced electrocatalytic activity for oxygen evolution. Angewandte Chemie International Edition, 56(14), 3897-3900. doi:10.1002/anie.201612635

https://hdl.handle.net/10356/138645

https://doi.org/10.1002/anie.201612635

Carbon Incorporated Ni-Co Mixed Metal Phosphides Nanoboxes with Enhanced Electrocatalytic Activity for Oxygen Evolution

*Peilei He, Xin-Yao Yu and Xiong Wen (David) Lou**

[*] Dr. P. He, Dr. X. Y. Yu, Prof. X. W. Lou

School of Chemical and Biomedical Engineering, Nanyang Technological University, 62 Nanyang Drive, Singapore 637459 (Singapore)

Email: xwlou@ntu.edu.sg; Webpage: http://www.ntu.edu.sg/home/xwlou/

Abstract

Hollow nanostructures have attracted increasing research interest in electrochemical energy storage and conversion owing to their unique structural features. However, the synthesis of hollow nanostructured metal phosphides, especially nonspherical hollow nanostructure, is rarely reported. Herein, we develop a metal-organic frameworks (MOFs)-engaged strategy to synthesize carbon incorporated Ni-Co mixed metal phosphide nanoboxes (denoted as NiCoP/C). Oxygen evolution reaction (OER) is selected as a demonstration to investigate the electrochemical performance of the NiCoP/C nanoboxes. For comparison, Ni-Co layered double hydroxide (Ni-Co LDH) and Ni-Co mixed metal phosphides (denoted as NiCoP) nanoboxes have also been synthesized. Benefiting from their structural and compositional merits, the as-synthesized NiCoP/C nanoboxes exhibit excellent electrocatalytic activity and long-term stability for OER.

Keywords: nanoboxes; metal phosphides; MOFs; electrocatalysis.

Controlled synthesis of nanostructures has drawn continuous attention, owing to the unique properties arising from their novel structure.[1-5] Amongst the myriad nanostructures, hollow nanostructures are of great interest because of their structural merits and have shown potential applications in various fields in recent years.[6-10] In particular, hollow nanostructures with higher surface-to-volume ratios and unique structural features hold great promise as electrode materials for electrochemical energy conversion and storage.[9, 11-14] For example, we have recently reported the synthesis of nickel and cobalt incorporated MoS_2 nanoboxes which exhibit excellent electrochemical performance for hydrogen evolution reaction (HER).[15]

Nanostructured metal phosphides have been intensively studied in recent years owing to their intriguing performance for applications in electrocatalysis,[16] photocatalysis,[17-18] lithium-ion[19-21] and sodium-ion[21-23] batteries. Especially, metal phosphides have been demonstrated to be promising electrocatalysts for HER.[24-27] For example, Feng et al. have synthesized porous nickel cobalt phosphides nanocubes via a template-engaged strategy using Prussian blue analogue as precursors.[26] They found that the synergistic effect between the two phases (Ni_2P and CoP) has great contribution to the excellent HER performance, which suggests that metal phosphides with complex compositions may improve the electrocatalytic activity compared to single phase metal phosphides. Meanwhile, metal phosphides have also been reported as a promising class of electrocatalysts for OER.[28-30] Although some progress has been made, the OER performance of metal phosphides needs to be further improved. Compared to solid nanostructures, hollow nanostructures could provide more active sites for electrochemical reactions. Therefore, enhanced electrocatalytic activities can be expected for hollow nanostructured metal phosphides with properly designed compositions.

Herein, we report a designed synthesis of nanocomposite nanoboxes containing Ni-Co mixed

metal phosphides and amorphous carbon (denoted as NiCoP/C nanoboxes) through a MOFs-engaged strategy. The synthesis process is schematically shown in **Figure 1**. Uniform Co-based zeolitic imidazolate framework (ZIF-67) nanocubes are synthesized through a surfactant-mediated method.[31] Then the collected ZIF-67 nanocubes are reacted with $Ni(NO_3)_2$ at room temperature to form Ni-Co LDH on the surface of ZIF-67 nanocubes. During the process, the inner part of ZIF-67 diffuses out of the nanocubes to form ZIF-67@LDH nanoboxes. Finally, these ZIF-67@LDH nanoboxes are chemically converted into Ni-Co mixed metal phosphides by reacting with NaH_2PO_2 at 350 ºC for 2 h in nitrogen atmosphere. At the same time, the organic ligands in ZIF-67 are transformed to amorphous carbon. As a result, unique NiCoP/C nanoboxes composed of Ni-Co mixed metal phosphides and amorphous carbon are obtained. The nanocomposite NiCoP/C nanoboxes exhibit enhanced electrochemical performance as an electrocatalyst for OER.

The morphology of the as-synthesized nanocubes is characterized by field-emission scanning electron microscopy (FESEM) and transmission electron microscopy (TEM). The FESEM image (Figure S1a, Supporting Information (SI)) indicates that the obtained nanocubes are highly uniform with a size of about 750 nm. A higher magnification FESEM image (Figure S1b, SI) reveals that the nanocubes have smooth surface. TEM images (Figure S1c,d, SI) verify the solid nature of the nanocubes. And the powder X-ray diffraction (XRD) pattern (Figure S2, SI) confirms the formation of phase-pure ZIF-67 nanocubes.[31] After reacting with an appropriate amount of $Ni(NO_3)_2$ for 90 min at room temperature, the solid ZIF-67 nanocubes are converted to nanoboxes. Typical FESEM images (**Figure 2**a,b) of the as-formed product indicate that the particles still keep the cubic morphology and size of the precursor ZIF-67 nanocubes but show rough surfaces. TEM images (Figure 2c,d) unambiguously reveal that the surface of the nanoboxes is assembled by nanosheets. The hollow interior of the nanoboxes can be observed by the contrast between the shell and the

inner void of nanoboxes. And the thickness of the shell is about 60 nm (Figure 2d). The XRD pattern is almost the same with that of ZIF-67 (Figure S2, SI), indicating the nanoboxes still contain ZIF-67. Energy dispersive X-ray (EDX) spectrum (Figure S3a, SI) reveals the existence of Ni element, evidencing the incorporation of Ni into the nanoboxes. In order to determine the composition of the nanoboxes, the residual ZIF-67 in the nanoboxes can be selectively removed. After reacting with water at 85 ºC, the product inherits the morphology of nanoboxes (Figure S4a-c, SI). The EDX spectrum (Figure S3b, SI) confirms the existence of Ni and Co elements. The XRD pattern (Figure S4d, SI) reveals the Ni-Co LDH phase of the product[32-33] and the disappearance of ZIF-67. These nanoboxes are also assembled by nanosheets (Figure S4c, SI). Therefore, the nanoboxes in Figure 2 are denoted as ZIF-67@LDH nanoboxes and the nanoboxes without ZIF-67 (Figure S4, SI) are denoted as Ni-Co LDH nanoboxes. EDX mapping images and line scan of a ZIF-67@LDH nanobox confirm that the NiCo-LDH is mainly located in the outer shell, while ZIF-67 is mainly located in the inner shell (Figure S5, SI).

In the synthesis of ZIF-67@LDH nanoboxes, ultrasonication is applied to obtain good dispersion of the ZIF-67@LDH particles (Figure S6, SI). Furthermore, when smaller ZIF-67 nanocubes (Figure S7a,b, SI) with a size of about 450 nm are used as the precursor and template, smaller ZIF-67@LDH nanoboxes with similar structure (Figure S7c,d, SI) can be obtained after reacting with $Ni(NO_3)_2$ for a much shorter time of 20 min. To investigate the structural evolution from ZIF-67 nanocubes to ZIF-67@LDH nanoboxes, time-dependent experiments are carried out. The intermediate products at different reaction times are collected and analyzed by FESEM and TEM (Figure S8, SI). When the reaction time is 30 min, small nanosheets grow on the surface of ZIF-67 nanocubes while the ZIF-67 nanocubes are still solid with rough surface (Figure S8a,d, SI). The nanosheets on the surface become larger and the voids appear inside the nanocubes after

reaction for 90 min (Figure S8b, e, SI). When the reaction time is prolonged to 120 min, the morphology of the product does not change significantly (Figure S8c, SI). The TEM image (Figure S8f, SI) reveals that the contrast between the shell and the void is much higher and some shells are broken. This observation indicates that the inner ZIF-67 in the nanocubes is totally etched away (Figure S8c,f, SI). The mechanism of the nanobox formation can be described as follows. When $Ni(NO_3)_2$ is added into the solution of ZIF-67, protons generated from the hydrolysis of Ni^{2+} will etch the ZIF-67 nanocubes. The Co^{2+} ions released from ZIF-67 are partially oxidized by O_2 and NO_3^- ions.[34] Meanwhile, the amount of hydroxyl ions increases with the consumption of protons. Then the Co^{2+}/Co^{3+} ions co-precipitate with Ni^{2+} ions to form a layer of LDH around the ZIF-67 nanocubes. As the reaction progresses, the inner ZIF-67 becomes vulnerable and the outward flow of Co^{2+} ions continues, which eventually leads to formation of nanoboxes.

After the phosphidation of ZIF-67@LDH, FESEM image (**Figure 3**a) shows that the morphology of nanoboxes is well maintained but nanosheets on the surface become nanoparticles (Figure 3b). Figure 3c clearly shows the cubic cavities inside the nanoboxes and a porous structure of the nanoboxes. The high angle annular dark field scanning transmission electron microscopy (HAADF-STEM) image (Figure 3d) of one single nanobox confirms its rough and porous feature. The EDX elemental mapping images (Figure 3e-g) confirm the even distribution of Ni, Co, and P elements throughout the whole shell of the nanobox. The XRD pattern (Figure S9, SI) shows that the product is composed of a mixture of CoP (JCPDS no. 65-2593) and Ni_2P (JCPDS no. 65-1989) with CoP as the major component. And the D-band (1350 cm^{-1}) and G-band (1580 cm^{-1}) peaks in the Raman spectrum (Figure S10, SI) demonstrate the existence of carbon in the nanoboxes. X-ray photoelectron spectroscopy (XPS) measurements further confirm the existence of Ni, Co, P, C, N and O elements in the products (Figure S11a, SI). The existence of O element may arise from the

superficial oxidation of NiCoP/C nanoboxes as a result of air contact.[35] As shown in the high-resolution XPS spectra, the peak around 852.8 eV in the Ni $2p_{3/2}$ spectrum (Figure S11b, SI) corresponds to Ni in Ni_2P and the peak around 778.6 eV in the Co $2p_{3/2}$ spectrum (Figure S11c, SI) is attributed to Co in CoP.[26] The P species with binding energy of 129.4 eV can be assigned to P bonded to Ni or Co (Figure S11d, SI). In the high-resolution XPS spectrum (Figure S11e, SI), the C 1s peaks at 284.8, 286.2, and 288.8 eV can be assigned to carbon in the form of C-C, C-O, and O=C-O, respectively,[36] and the C-C peak is far more dominant. Therefore, the as-synthesized product after phosphidation of the ZIF-67@LDH nanoboxes is denoted as NiCoP/C nanoboxes.

In addition, phosphidation of the Ni-Co LDH nanoboxes is also carried out at the same conditions. FESEM and TEM images of the product (Figure S12, SI) indicate a similar structure with that of the NiCoP/C nanoboxes. The XRD diffraction peaks are almost exactly the same to those of the NiCoP/C nanoboxes (Figure S9, SI), indicating this product is also composed of a mixture of CoP and Ni_2P. But there is no obvious peak observed between 1000 cm^{-1} and 2000 cm^{-1} in the Raman spectrum (Figure S10, SI) indicating absence of carbon in this product. Therefore, the product obtained by phosphidation of the Ni-Co LDH nanoboxes is denoted as NiCoP nanoboxes. Compared with NiCoP/C nanoboxes (Figure 3a), the NiCoP nanoboxes (Figure S12a, SI) are more fragile. Clearly, the existence of carbon in NiCoP/C nanoboxes improves the structural stability of the nanoboxes. EDX spectra of both NiCoP/C and NiCoP samples confirm the existence of Ni, Co, and P elements (Figure S13, SI).

The electrocatalytic activity of the as-synthesized three samples (Ni-Co LDH, NiCoP, and NiCoP/C) is investigated as electrocatalysts for OER. **Figure 4**a shows the polarization curves with IR correction. It can be seen that the NiCoP/C nanoboxes show the lowest onset potential and highest current density for OER. The operating potentials required at a current density of 10 mA

cm^{-2} are compared (a metric associated with solar fuel synthesis[37]). To obtain a current density of 10 mA cm^{-2}, the NiCoP/C nanoboxes require an overpotential of 330 mV, which is comparable to the performance of many other metal phosphides-based catalysts (Table S1, SI) and lower than that of NiCoP nanoboxes (370 mV) and Ni-Co LDH nanoboxes (420 mV). The Tafel plots of the NiCoP/C, NiCoP and Ni-Co LDH nanoboxes are shown in Figure 4b. The Tafel slope of 96 mV dec^{-1} for NiCoP/C nanoboxes is much lower than 115 mV dec^{-1} for NiCoP nanoboxes and 135 mV dec^{-1} for Ni-Co LDH nanoboxes, implying the favorable OER kinetics for NiCoP/C nanoboxes.

The electrochemical active surface area (ECSA) is in proportion to the electrochemical double-layer capacitance (C_{dl}).[38-39] Therefore, to estimate the ECSA, C_{dl} is calculated by measuring the cyclic voltammetry (CV) curves in the proper potential range without redox processes (Figure S14, SI). The NiCoP/C nanoboxes have much larger C_{dl} (146 mF cm^{-2}) than the Ni-Co LDH nanoboxes (9.15 mF cm^{-2}) and NiCoP nanoboxes (28.93 mF cm^{-2}), suggesting the highest electrocatalytic activity of the NiCoP/C nanoboxes. Furthermore, electrochemical impedance spectroscopy (EIS) analysis is performed to study the interfacial properties of the as-obtained electrocatalysts modified electrodes (Figure S15, SI). As can be seen, the electron-transfer resistance of NiCoP/C is much lower than that of Ni-Co LDH and NiCoP nanoboxes, which may be another reason for the enhanced electrocatalytic performance. Lastly, the stability of the three electrocatalysts is investigated at 1.58 V (Figure 4c). Remarkably, 96.5% of the initial current is retained after 10 h for the NiCoP/C nanoboxes, whereas the current losses of NiCoP nanoboxes (13%) and Ni-Co LDH nanoboxes (40%) are much higher. All of these results demonstrate that the NiCoP/C nanoboxes possess superior OER activity as well as good stability. And the mechanism of the NiCoP/C nanoboxes for OER may be consistent with the reported mechanism.[40] Ni and Co cations on the surface are partially oxidized into NiOOH and CoOOH and

form Ni_2P/NiOOH and CoP/CoOOH core-shell structures as the actual surface-active sites.[40] The enhanced electrocatalytic activity of NiCoP/C nanoboxes for OER might be attributed to the following aspects. First, a synergistic combination of different metal phosphides in the nanocomposite may contribute to the enhanced electrocatalytic activity and the existence of carbon is expected to improve the charge transfer efficiency and conductivity. Second, the NiCoP/C nanoboxes with a porous structure can provide more active sites for the catalytic process. Moreover, the hollow structure with high specific surface area can endow more electrolyte/electrode contact area for the electrochemical reaction.

In summary, we have developed a facile metal-organic frameworks (MOFs)-engaged strategy to synthesize NiCoP/C, NiCoP, and Ni-Co LDH nanoboxes as electrocatalysts for OER from ZIF-67 nanocubes precursors. With their structural and compositional advantages, the NiCoP/C nanoboxes show much more enhanced electrocatalytic activity for OER than NiCoP and Ni-Co LDH nanoboxes. Specifically, the NiCoP/C nanoboxes require an overpotential as low as 330 mV to attain a current density of 10 mA cm^{-2}. In addition, the NiCoP/C nanoboxes show better long-term stability than NiCoP nanoboxes and Ni-Co LDH nanoboxes under the same operating conditions. This work represents an important addition to the growing family of MOFs-derived functional materials for various applications.

Acknowledgements

X. W. L. acknowledges the funding support from the National Research Foundation (NRF) of Singapore via the NRF investigatorship (NRF-NRFI2016-04).

References

[1] Z. X. Wu, W. Li, P. A. Webley, D. Y. Zhao, *Adv. Mater.* **2012**, *24*, 485.

[2] T. T. Zhuang, Y. Liu, M. Sun, S. L. Jiang, M. W. Zhang, X. C. Wang, Q. Zhang, J. Jiang, S. H. Yu, *Angew. Chem. Int. Ed.* **2015**, *54*, 11495.

[3] H. L. Liu, F. Nosheen, X. Wang, *Chem. Soc. Rev.* **2015**, *44*, 3056.

[4] B. Y. Guan, L. Yu, X. W. Lou, *J. Am. Chem. Soc.* **2016**, *138*, 11306.

[5] L. H. Hu, Q. Peng, Y. D. Li, *J. Am. Chem. Soc.* **2008**, *130*, 16136.

[6] X. Y. Yu, L. Yu, X. W. Lou, *Adv. Energy Mater.* **2016**, *6*, 1501333.

[7] J. Liu, H. Q. Yang, F. Kleitz, Z. G. Chen, T. Y. Yang, E. Strounina, G. Q. Lu, S. Z. Qiao, *Adv. Funct. Mater.* **2012**, *22*, 591.

[8] X. W. Lou, L. A. Archer, Z. C. Yang, *Adv. Mater.* **2008**, *20*, 3987.

[9] P. P. Wang, H. Y. Sun, Y. J. Ji, W. H. Li, X. Wang, *Adv. Mater.* **2014**, *26*, 964.

[10] Z. Li, H. B. Wu, X. W. Lou, *Energy Environ. Sci.* **2016**, *9*, 3061.

[11] B. Y. Guan, L. Yu, X. W. Lou, *Adv. Mater.* **2016**, *28*, 9596.

[12] X. Y. Yu, L. Yu, H. B. Wu, X. W. Lou, *Angew. Chem. Int. Ed.* **2015**, *54*, 5331.

[13] X. B. Xu, F. Nosheen, X. Wang, *Chem. Mater.* **2016**, *28*, 6313.

[14] J. L. Liu, Y. Yang, B. Ni, H. Y. Li, X. Wang, *Small* **2017**, *13*, 1602637.

[15] X. Y. Yu, Y. Feng, Y. Jeon, B. Y. Guan, X. W. Lou, U. Paik, *Adv. Mater.* **2016**, *28*, 9006.

[16] Y. M. Shi, B. Zhang, *Chem. Soc. Rev.* **2016**, *45*, 1529.

[17] J. F. Callejas, J. M. McEnaney, C. G. Read, J. C. Crompton, A. J. Biacchi, E. J. Popczun, T. R. Gordon, N. S. Lewis, R. E. Schaak, *ACS Nano* **2014**, *8*, 11101.

[18] Q. D. Yue, Y. Y. Wan, Z. J. Sun, X. J. Wu, Y. P. Yuan, P. W. Du, *J. Mater. Chem. A* **2015**, *3*, 16941.

[19] G. H. Li, H. Yang, F. C. Li, J. Du, W. Shi, P. Cheng, *J. Mater. Chem. A* **2016**, *4*, 9593.

[20] X. Wang, H.-M. Kim, Y. Xiao, Y.-K. Sun, *J. Mater. Chem. A* **2016**, *4*, 14915.

[21] M. Sun, H. J. Liu, J. H. Qu, J. H. Li, *Adv. Energy Mater.* **2016**, *6*, 1600087.

[22] J. F. Qian, Y. Xiong, Y. L. Cao, X. P. Ai, H. X. Yang, *Nano Lett.* **2014**, *14*, 1865.

[23] Y. J. Kim, Y. Kim, A. Choi, S. Woo, D. Mok, N.-S. Choi, Y. S. Jung, J. H. Ryu, S. M. Oh, K. T. Lee, *Adv. Mater.* **2014**, *26*, 4139.

[24] G. F. Chen, T. Y. Ma, Z. Q. Liu, N. Li, Y. Z. Su, K. Davey, S. Z. Qiao, *Adv. Funct. Mater.* **2016**,

26, 3314.

[25] J. Yang, F. J. Zhang, X. Wang, D. S. He, G. Wu, Q. H. Yang, X. Hong, Y. E. Wu, Y. D. Li, *Angew. Chem. Int. Ed.* **2016**, *55*, 12854.

[26] Y. Feng, X. Y. Yu, U. Paik, *Chem. Commun.* **2016**, *52*, 1633.

[27] Y. J. Li, H. C. Zhang, M. Jiang, Y. Kuang, X. M. Sun, X. Duan, *Nano Res.* **2016**, *9*, 2251.

[28] X. Y. Yu, Y. Feng, B. Y. Guan, X. W. Lou, U. Paik, *Energy Environ. Sci.* **2016**, *9*, 1246.

[29] D. Li, H. Baydoun, C. N. Verani, S. L. Brock, *J. Am. Chem. Soc.* **2016**, *138*, 4006.

[30] L.-A. Stern, L. G. Feng, F. Song, X. L. Hu, *Energy Environ. Sci.* **2015**, *8*, 2347.

[31] H. Hu, B Y. Guan, X W. Lou, *Chem* **2016**, *1*, 102.

[32] Z. Jiang, Z. P. Li, Z. H. Qin, H. Y. Sun, X. L. Jiao, D. R. Chen, *Nanoscale* **2013**, *5*, 11770.

[33] G. L. Fan, F. Li, D. G. Evans, X. Duan, *Chem. Soc. Rev.* **2014**, *43*, 7040.

[34] H. Hu, B. Y. Guan, B. Y. Xia, X. W. Lou, *J. Am. Chem. Soc.* **2015**, *137*, 5590.

[35] Q. Liu, J. Q. Tian, W. Cui, P. Jiang, N. Y. Cheng, A. M. Asiri, X. P. Sun, *Angew. Chem. Int. Ed.* **2014**, *53*, 6710.

[36] Y. Li, Y. Zhao, H. H. Cheng, Y. Hu, G. Q. Shi, L. M. Dai, L. T. Qu, *J. Am. Chem. Soc.* **2012**, *134*, 15.

[37] T. Y. Ma, S. Dai, M. Jaroniec, S. Z. Qiao, *J. Am. Chem. Soc.* **2014**, *136*, 13925.

[38] C. C. L. McCrory, S. Jung, J. C. Peters, T. F. Jaramillo, *J. Am. Chem. Soc.* **2013**, *135*, 16977.

[39] H. B. Wu, B. Y. Xia, L. Yu, X. Y. Yu, X. W. Lou, *Nat. Commun.* **2015**, *6*, 6512.

[40] G. Zhang, G. C. Wang, Y. Liu, H. J. Liu, J. H. Qu, J. H. Li, *J. Am. Chem. Soc.* **2016**, *138*, 14686.

Figures and captions

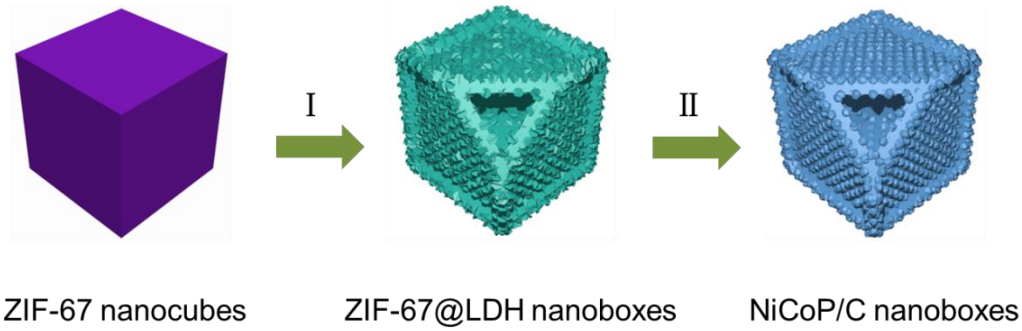

Figure 1. Schematic illustration of the formation process of NiCoP/C nanoboxes: (Ⅰ) reaction of ZIF-67 nanocubes with $Ni(NO_3)_2$ to form ZIF-67@LDH nanoboxes and (Ⅱ) phosphidation of ZIF-67@LDH nanoboxes to obtain NiCoP/C nanoboxes.

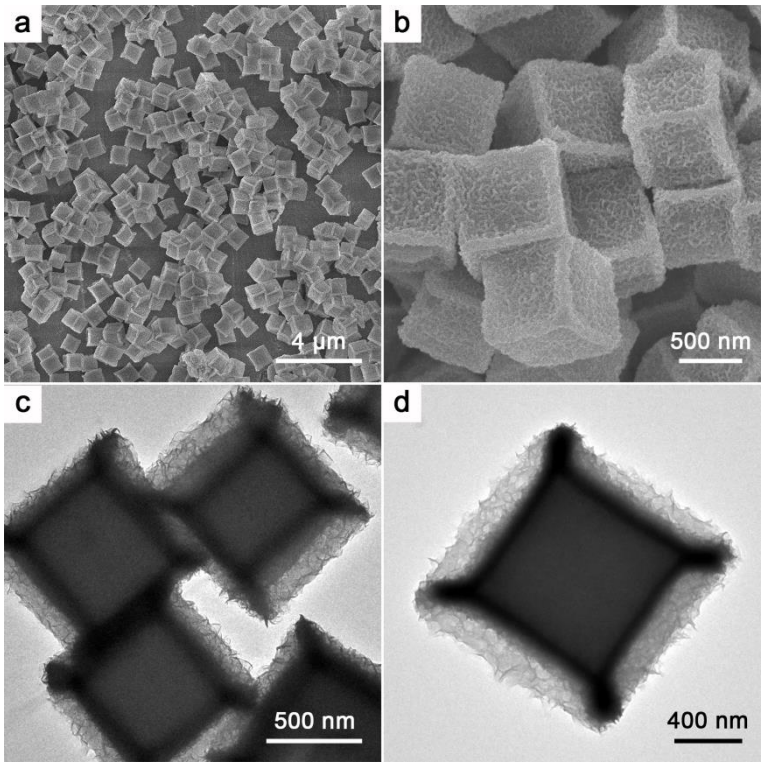

Figure 2. (a,b) FESEM and (c,d) TEM images of ZIF-67@LDH nanoboxes synthesized by reacting ZIF-67 nanocubes with $Ni(NO_3)_2$ at 25 ºC for 90 min.

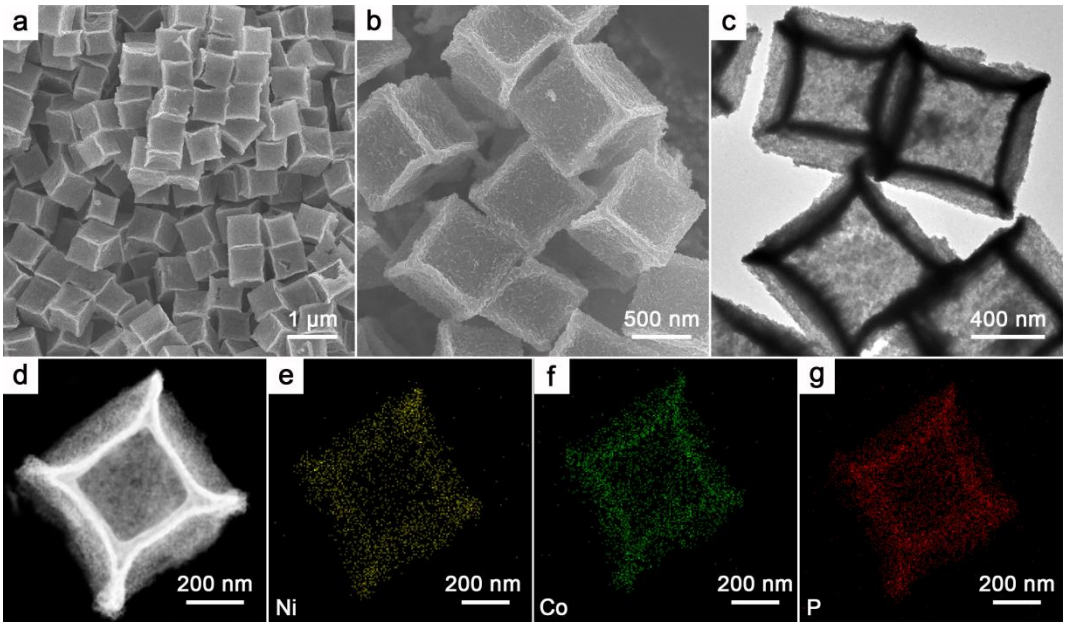

Figure 3. (a,b) FESEM images, (c) TEM image and (d) HAADF-STEM image of the NiCoP/C nanoboxes. Elemental mapping images of Ni (e), Co (f), and P (g) of an individual nanobox.

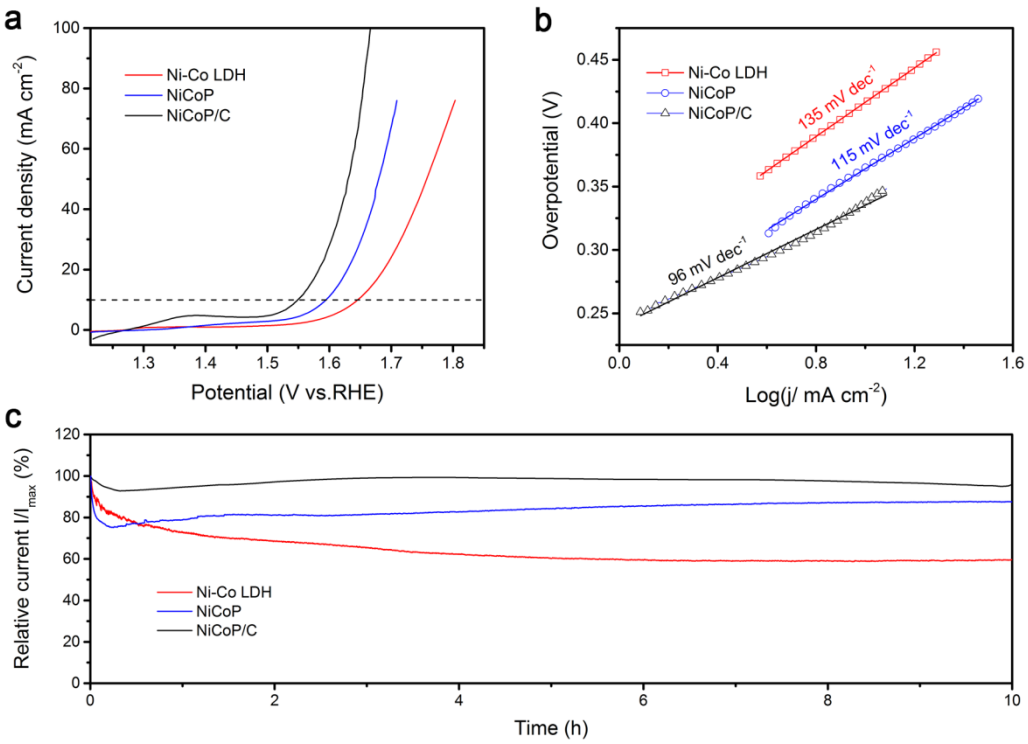

Figure 4. (a) Polarization curves, (b) Tafel plots, and (c) chronoamperometry curves of Ni-Co LDH, NiCoP and NiCoP/C nanoboxes in an O_2-saturated 1.0 M KOH solution.

for Table of Content Entry

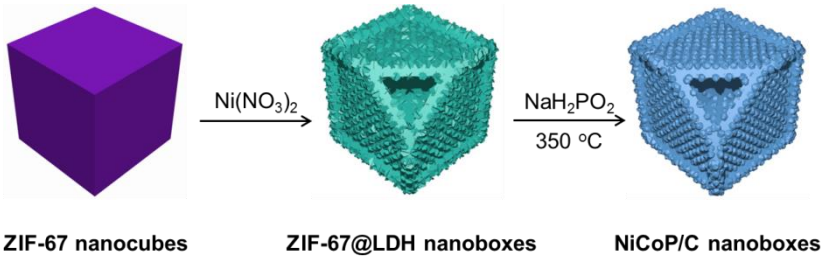

ZIF-67@LDH nanoboxes are synthesized from highly uniform ZIF-67 nanocubes through reacting with $Ni(NO_3)_2$ at room temperature. After phosphidation with NaH_2PO_2, the ZIF-67@LDH nanoboxes are transformed into NiCoP/C nanoboxes, which manifest enhanced electrocatalytic performance as an electrocatalyst for the oxygen evolution reaction.